Supplementary Information

Multi-Moiré Networks in Engineered Lateral Hetero-Bilayers: Programmable Phononic Reconfiguration and Second Harmonic Generation

Suman Kumar Chakraborty[1], Frederico B. Sousa[2], Chakradhar Sahoo[3], Indrajeet Dhananjay Prasad[4], Shneha Biswas[5], Purbasha Ray[1], Biswajeet Nayak[1], Rafael Rojas[2], Baisali Kundu[1], Alfred J. H. Jones[3], Jill A. Miwa[3], Søren Ulstrup[3], Sudipta Dutta[5], Santosh Kumar[4], Leandro M. Malard[2], Gopal K. Pradhan[6], Prasana Kumar Sahoo[1]*

[1]Quantum Materials and Device Research lab, Materials Science Centre, Indian Institute of Technology Kharagpur, West Bengal, India
[2]Departamento de Física, Universidade Federal de Minas Gerais, Belo Horizonte,Brazil
[3]Department of Physics and Astronomy, Interdisciplinary Nanoscience Center, Aarhus University, 8000 Aarhus C, Denmark
[4]Department of Physics, Indian Institute of Technology Goa, Goa, India
[5]Department of Physics, Indian Institute of Science Education and ResearchTirupati, Andhra Pradesh, India
[6]Department of Physics, School of Applied Sciences, KIIT Deemed to be University, Bhubaneswar, India

**prasana@matsc.iitkgp.ac.in*

Table of Contents

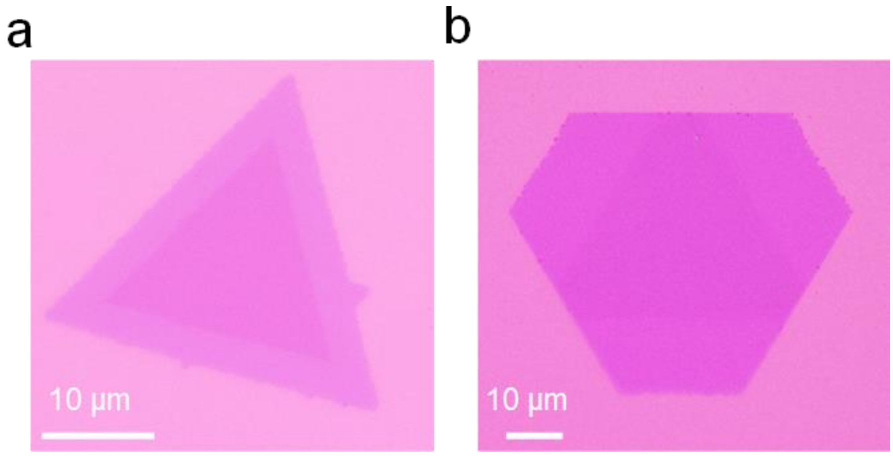

Figure S1. Optical Microscope images of monolayer (a) $MoSe_2$-WSe_2 and (b) MoS_2-WS_2 lateral heterostructures.

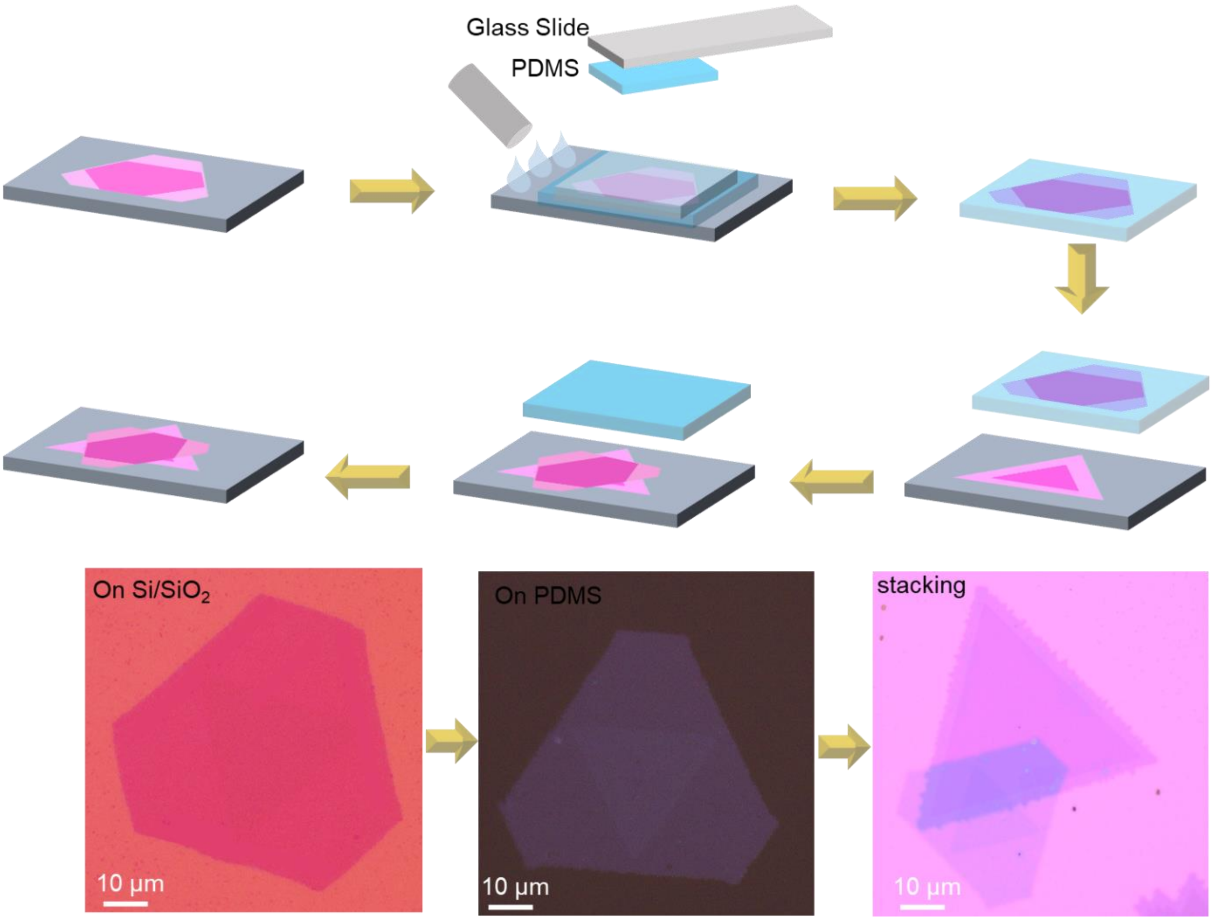

Figure S2. Schematic representation of the water-assisted transfer strategy for the fabrication of hetero-bilayers of lateral hetero-monolayers.

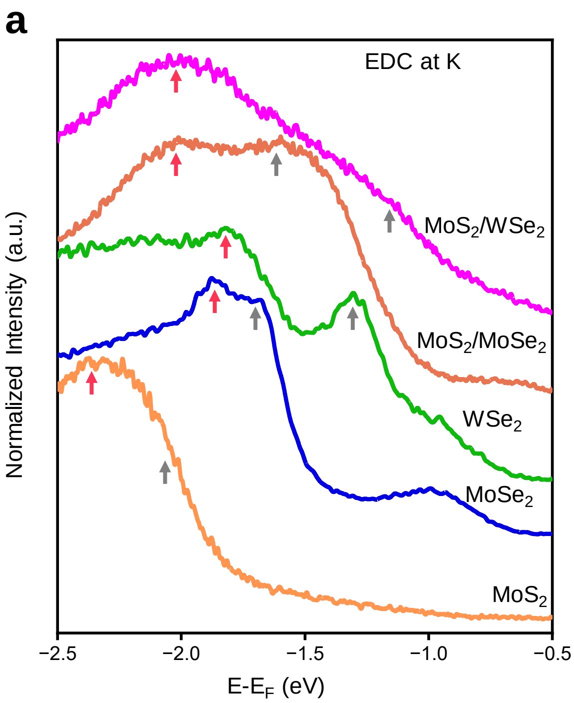

b

Material	VB_1 (eV)	VB_2 (eV)
MoS_2	-2.1129	-2.332
$MoSe_2$	-1.6687	-1.8544
WSe_2	-1.28544	-1.8078
$MoS_2/MoSe_2$	-1.486	-2.046
MoS_2/WSe_2	-1.3103	-1.9833

Figure S3. (a) Energy distribution curve (EDC) extracted at the K-point. (b) Fitted EDC peak positions using Lorentzian functions.

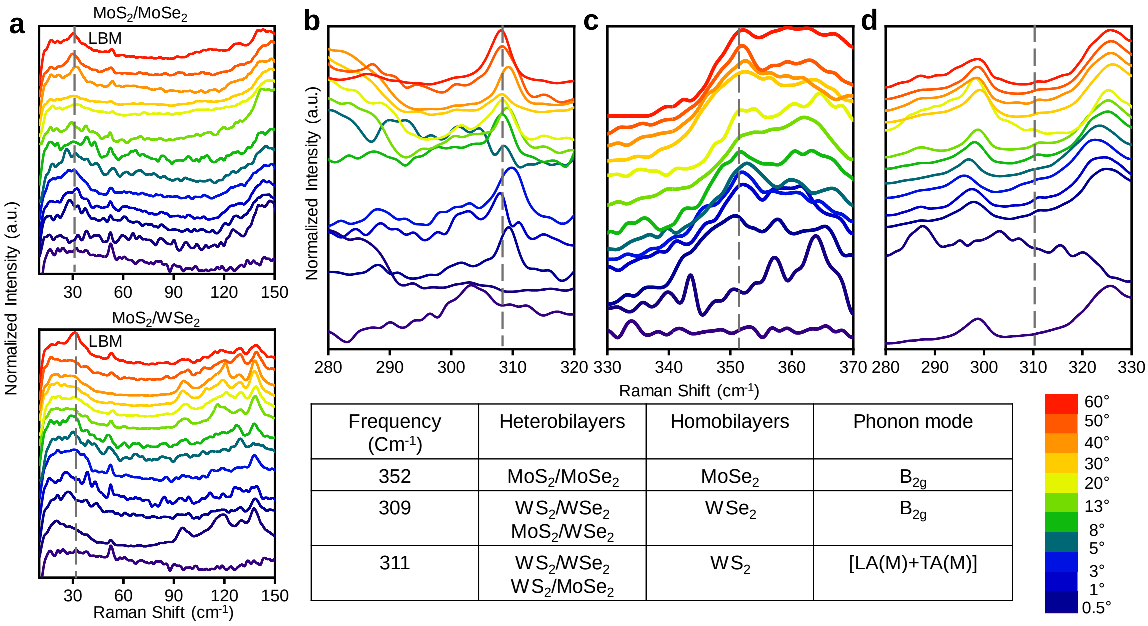

Frequency (Cm^{-1})	Heterobilayers	Homobilayers	Phonon mode
352	$MoS_2/MoSe_2$	$MoSe_2$	B_{2g}
309	WS_2/WSe_2 MoS_2/WSe_2	WSe_2	B_{2g}
311	WS_2/WSe_2 $WS_2/MoSe_2$	WS_2	[LA(M)+TA(M)]

Figure S4. Lower Breathing Mode of (a) $MoS_2/MoSe_2$ and MoS_2/WSe_2 moiré networks. (b-d) Signatures of interlayer coupling as activation of forbidden modes of monolayers into hetero-bilayers. The table shows different phone modes in the moiré system.

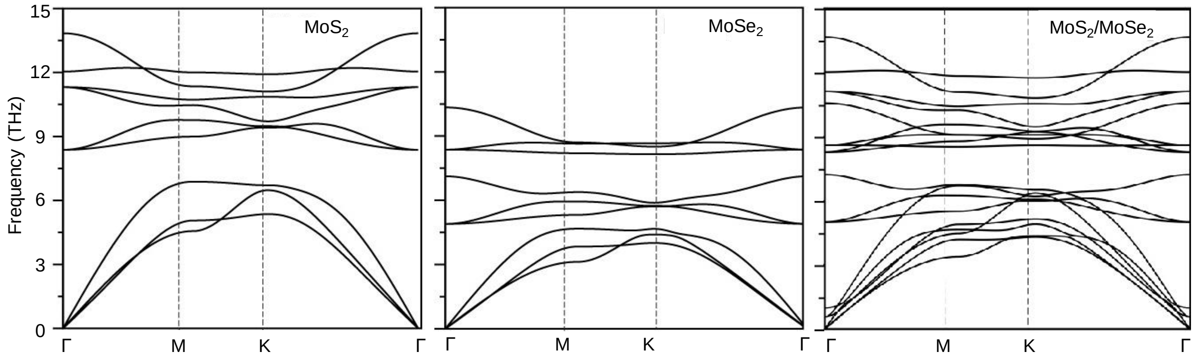

Figure S5. Simulated Phonon dispersion of monolayer MoS_2, $MoSe_2$ and $MoS_2/MoSe_2$.

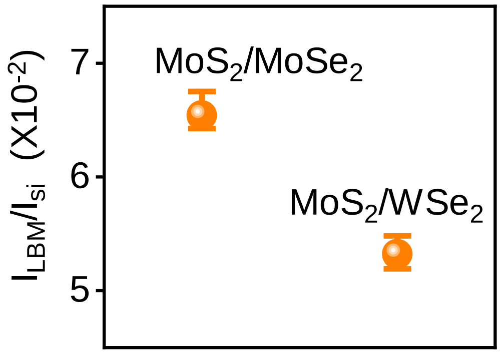

Figure S6. Strength of interlayer coupling: as the transition metal changes, the coupling strength decreases.

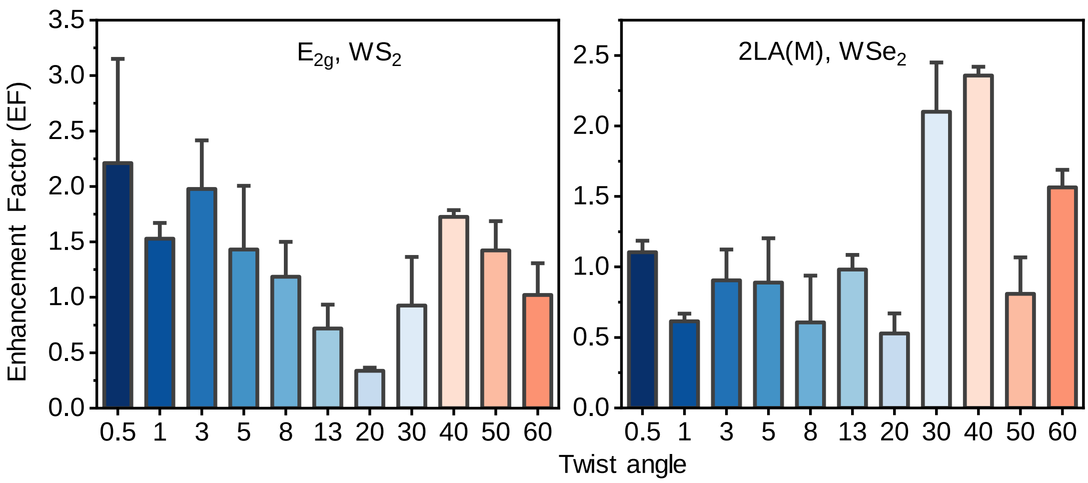

Figure S7. Resonant Raman Process of in-plane phonon modes of WS_2 and WSe_2 in WS_2/WSe_2.

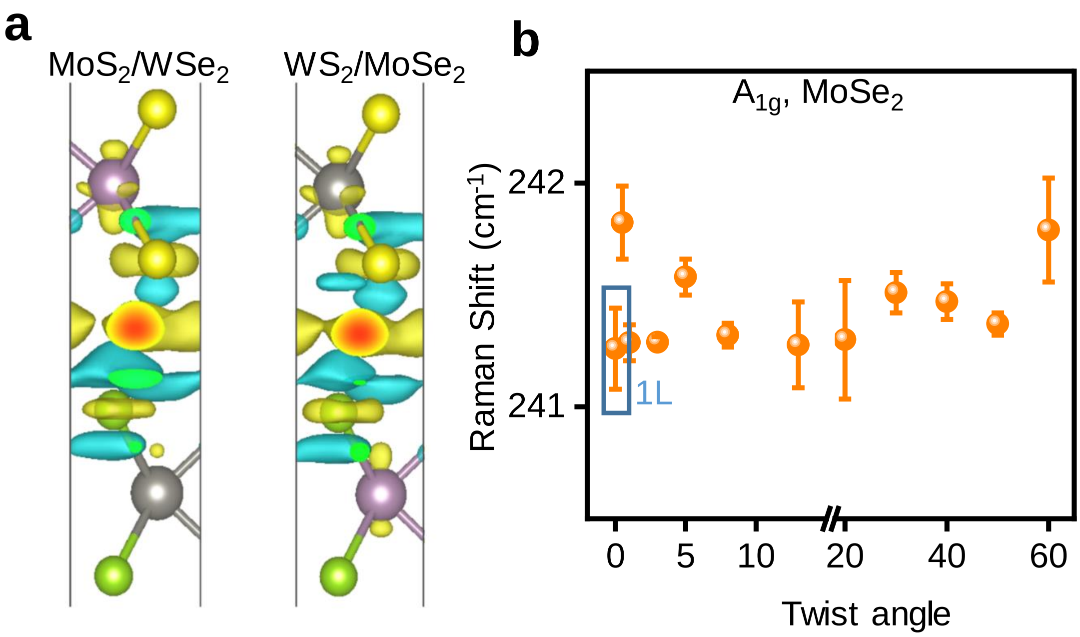

Figure S8. (a) Differential charge density of MoS_2/WSe_2 and $WS_2/MoSe_2$. (b) A_{1g} mode peak position variation of $MoSe_2$ in $MoS_2/MoSe_2$ compared to 1L. Blue shift of $MoSe_2$ indicates electron transfer from $MoSe_2$ to MoS_2.

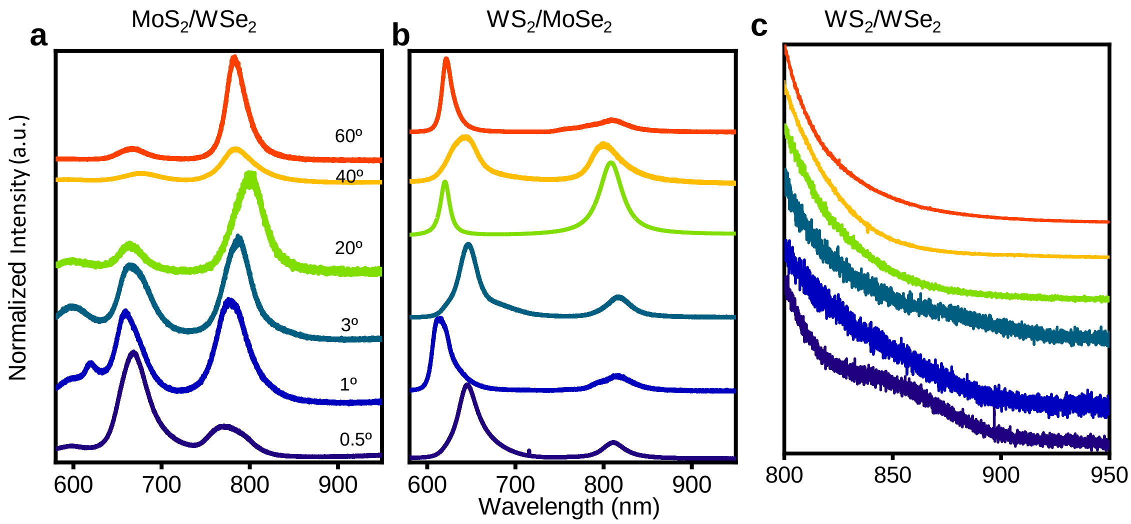

Figure S9. (a, b) Intralayer *A* (X_0) exciton intensity variation. (c) Interlayer exciton profile for WS_2/WSe_2. The presence of interlayer exciton at 0.5º due to efficient charge transfer and higher PL quantum yield of WS_2 and WSe_2 at room temperature.

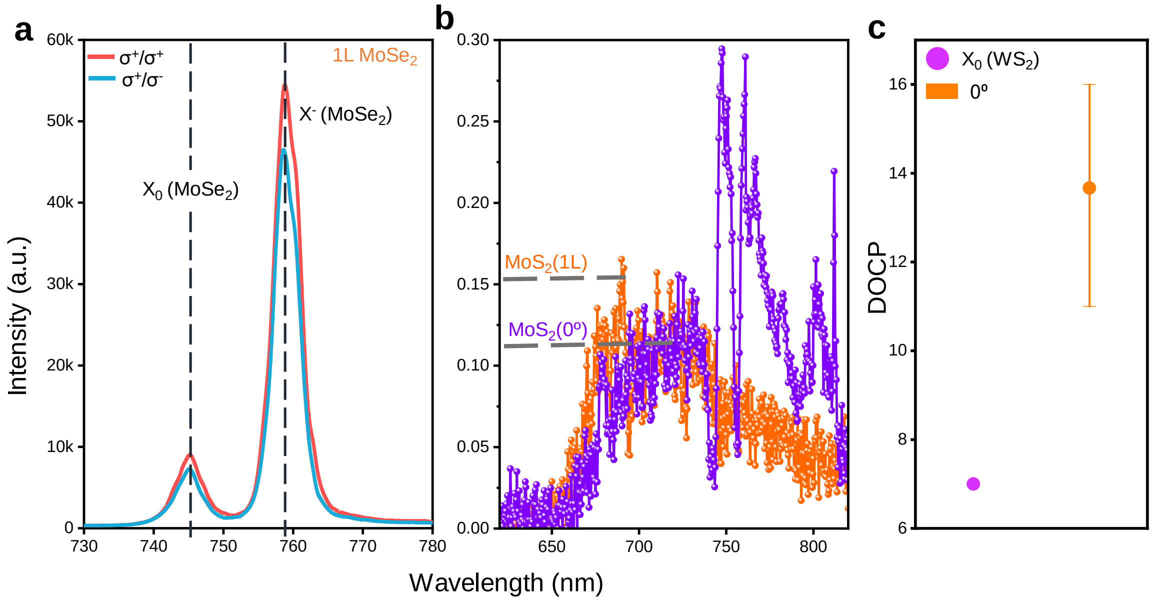

Figure S10. Low temperature (5K) PL spectra: (a) DOCP variation of intralayer exciton and trion of 1L $MoSe_2$ 1L, (b) DOCP of MoS_2 intralayer exciton in 1L to 0º stacked $MoS_2/MoSe_2$ heterobilayer. (C) WS_2 in 1L to WS_2/WSe_2 (0º). .

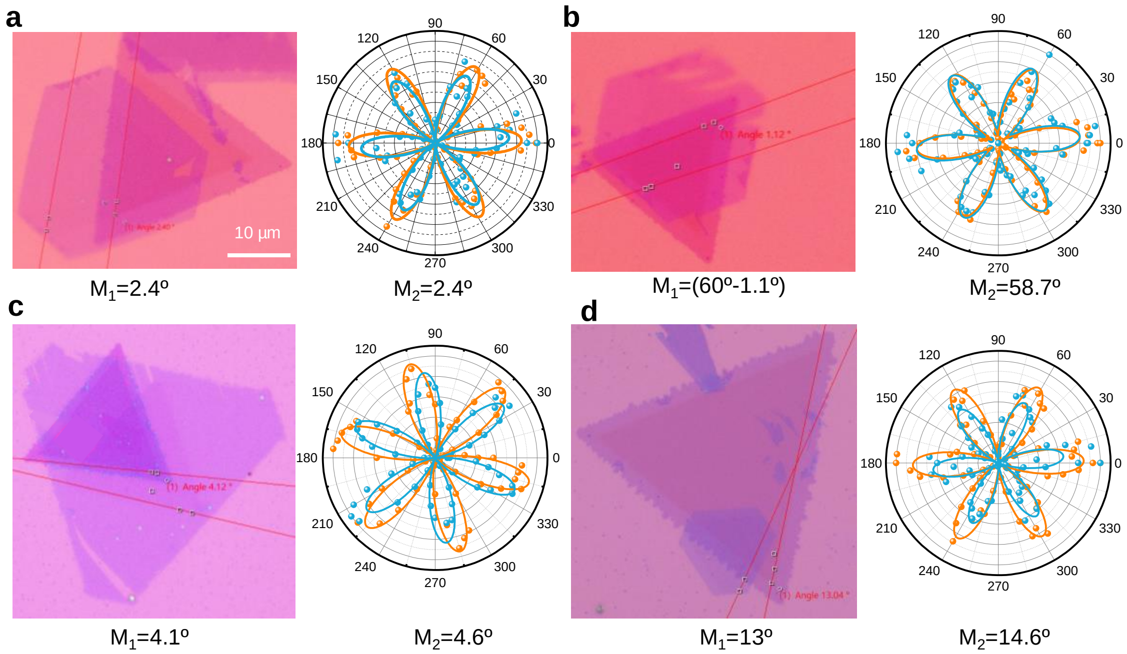

Figure S11. Polarization-resolved SHG measurements for identification of angles (M_1= angle measured from optical microscope image and OLYMPUS software, whereas M_2=measure angle from SHG)

Table S1: Shear-strength comparison of the four individual TMDs

Material	Young's Modulus (GPa)	Poisson's ratio	Shear strength (GPa)
WS_2	302	0.22	~123 (Ref.1)
WSe_2	258	0.19	~108 (Ref.1)
MoS_2	270	0.95	69 (Ref.2)
			~0.011 (Ref.3)
			25 (Ref.4)
$MoSe_2$	177	0.23	~72 (Ref.5)

$E=2G(1+Y)$, E=Mechanical modulus, G=Shear Modulus, Y=Poisson's ratio.

Table S2: Excitonic-resonances for the four individual TMDs

Material	A (X_o) (eV)	B (eV)	C (eV)	D (eV)
WS_2	1.97	2.34	2.82 (Ref.6,7)	
WSe_2	1.60	2.06	2.2	>2.9 (Ref.7,8)
MoS_2	1.83	1.98	2.86 (Ref.7,9,10)	
$MoSe_2$	1.52	1.68	2.52 (Ref.7)	

Table S3: Direct Interlayer-exciton transitions

Material	IX$(K\text{-}K)$ (eV)
WS_2/WSe_2	0.921
$MoS_2/MoSe_2$	0.778
MoS_2/WSe_2	0.623

References:

1. Falin, A. *et al.* Mechanical Properties of Atomically Thin Tungsten Dichalcogenides: WS_2, WSe_2, and WTe_2. *ACS Nano* 15, 2600–2610 (2021).
2. Bertolazzi, S., Brivio, J. & Kis, A. Stretching and Breaking of Ultrathin MoS_2. *ACS Nano* 5, 9703–9709 (2011).
3. Sun, Y. *et al.* Determining the interlayer shearing in twisted bilayer MoS_2 by nanoindentation. *Nat. Commun.* 13, 3898 (2022).
4. Oviedo, J. P. *et al.* In Situ TEM Characterization of Shear-Stress-Induced Interlayer Sliding in the Cross Section View of Molybdenum Disulfide. *ACS Nano* 9, 1543–1551 (2015).
5. Yang, Y. *et al.* Brittle Fracture of 2D $MoSe_2$. *Adv. Mater.* 29, 1604201 (2017).
6. Zhu, B., Chen, X. & Cui, X. Exciton Binding Energy of Monolayer WS2. *Sci. Rep.* 5, 9218 (2015).
7. Kozawa, D. *et al.* Photocarrier relaxation pathway in two-dimensional semiconducting transition metal dichalcogenides. *Nat. Commun.* 5, 4543 (2014).
8. Wang, K. *et al.* Interlayer Coupling in Twisted WSe_2/WS_2 Bilayer Heterostructures Revealed by Optical Spectroscopy. *ACS Nano* 10, 6612–6622 (2016).
9. Khatua, D. P. *et al.* A comparative study of ultrafast carrier dynamics near A, B, and C-excitons in a monolayer MoS_2 at high excitation densities. *Opt. Mater.* 126, 112224 (2022).
10. Wang, L. *et al.* Slow cooling and efficient extraction of C-exciton hot carriers in MoS_2 monolayer. *Nat. Commun.* 8, 13906 (2017).